FINITE ELEMENT ANALYSIS OF A BEAM WITH ACTIVE CONSTRAINED LAYER DAMPING (ACLD) TREATMENT+

Pankaj K. Langote* and P. Seshu**

Abstract

Active Constrained Layer Damping (ACLD) treatments with active piezoelectric materials and passive Visco-Elastic Materials (VEMs) combine the advantages of both conventional Active Damping (AD) and Passive Constrained Layer Damping (PCLD) treatments. A beam Finite Element (FE) model has been developed for the beam partially covered with ACLD treatments on both sides of beam. For modeling the frequency dependent damping behavior of the VEM, the Golla-Hughes-McTavish (GHM) model has been used. In all, four systems have been studied viz., bare beam, beam-piezo (AD), beam-VEM (PCLD), and beam-VEM-piezo (ACLD). A set of experiments has been conducted on all the systems. A very good match between theoretical and experimental predictions, in terms of free vibration response as well as closed loop feedback controlled dynamic response, has been established.

***Key words**: ACLD, FEM, experimental studies, GHM, PCLD.*

Nomenclature

$[A]$ = state-space system matrix
A_a, A_b, A_p, A_v = cross-sectional area of aluminum layer, beam, piezoelectric layer and viscoelastic layer
b = width for beam, aluminum layer, piezoelectric layer and VEM
$[C]$ = damping matrix
D = electrical displacement
d_{31} = piezoelectric constant
E = electric field
E_b, E_a, E_p = Young's Modulus of beam, aluminum and piezoelectric material
P_c = control force vector
f_d = disturbance force vector
$G(t)$ = relaxation function of VEM
G_o = final value of $G(t)$
I_b, I_a, I_p = moment of inertia of beam, aluminum and piezoelectric layers, respectively
K = global stiffness matrix
L = length of beam
L_e = element length
M = global mass matrix
$\{q\}$ = global displacement vector
t = time
t_a, t_b, t_p, t_v = thickness of aluminum layer, base beam, piezoelectric layer, and VEM, respectively
u_a, u_b, u_p, u_v = axial displacement of aluminum layer, beam, piezoelectric layer, and VEM, respectively
V = applied voltage
w = beam transverse displacement
x = position co-ordinate along beam and element length
z = dissipation coordinate
$\hat{\alpha}$ = weighing on GHM dissipation coordinate (related to loss factor)
γ = shear strain of viscoelastic material
$\hat{\zeta}$ = damping factor in GHM dissipation coordinate
ρ_a, ρ_b, ρ_p, ρ_v = mass density of aluminum layer, beam, piezoelectric layer, and VEM, respectively
ψ = rotational angle in VEM
$\hat{\omega}$ = natural frequency in GHM dissipation coordinate

* Scientist/Engineer, Structures Group, ISRO Satellite Centre, Airport Road, Vimanapura Post, Bangalore-560 017, India, Email : PankajLangote@yahoo.com
** Associate Professor, Department of Mechanical Engineering, Indian Institute of Technology Bombay, Powai, Mumbai-400 076, India, Email : seshu@me.iitb.ac.in
Manuscript received on 08 Mar 2004; Paper reviewed, revised and accepted on 27 Sep 2004

+ This research work was carried out by the first author as a part of his Master's Thesis work at Indian Institute of of Technology Bombay, Mumbai, India

Subscripts

a, b, p, v = aluminum, beam, piezoelectric, and VEM, respectively
le, te = leading, and trailing edge, respectively

Introduction

In the recent past, the use of damping treatments for vibration control of flexible structures has been well studied. To add passive damping to structures, viscoelastic materials (VEMs) are applied. In order to enhance the damping effect of the VEM, a passive constraining layer could be attached, creating a passive constrained layer damping (PCLD) treatment. When the constraining layer of the PCLD is an active element such as piezoelectric layer, the treatment is called active constrained layer damping (ACLD) treatment. If the active piezoelectric layer is directly used without a VEM layer, it becomes simple active damping (AD) treatment.

Baz [1] proposed a mathematical model to analyze the steady state vibration response of Euler-Bernoulli beams with ACLD treatments. He used distributed piezoelectric sensors to measure vibration response and a PD controller to actuate the piezoelectric actuator. Shen [2] derived an eighth-order matrix differential equation governing bending and axial vibrations of an ACLD treated beam to model the dynamics of ACLD. He presented numerical examples on a cantilever beam with fully covered ACLD and showed that ACLD could produce significant damping. To study three-layer sandwich beams, Van Nostrand and Inman [3] developed a finite element model with four degrees of freedom per node, for which they considered only transverse shear strain in the viscoelastic layer.

Rongong et. al. [4] proposed two treatments bonded symmetrically on the top and bottom surfaces of the beam. Their ACLD configuration had PZT actuator bonded to a stiff aluminum constraining layer which in turn was bonded to the structure by a thin viscoelastic layer. This construction had the advantage of allowing the lengths of the active and passive treatments to be different, in contrast to the preceding ACLD ones which required actuators entirely covering the viscoelastic layers. They proposed a model based on the Rayleigh-Ritz method. They also performed some experiments to validate their model using 3M ISD 112 viscoelastic damping layers, PZT actuators, and accelerometer sensors.

Shi et. al. [5] proposed a new model reduction procedure to reduce the size of final viscoelastic matrices. Balamurugan and Narayanan [6] developed a finite element model of three-layer sandwich beam taking into account shear deformation and rotary inertia. Lim et. al. [7] developed a three dimensional finite element closed-loop model to predict the effects of active passive damping on a vibrating structure. Comparisons among several ACLD models, passive and active damping models were made.

In all the studies, ACLD treatments have always been found to be more effective than passive ones. However, it has been found that these ACLD treatments suffer from loss of active action transmissibility from the piezoelectric actuator to the structure, due to the flexibility of the intermediate VEM layer. To remedy the transmissibility reduction problem, Liao and Wang [8] suggested enhanced ACLD by adding rigid edge elements at the edges or the actuators to connect them directly to the structure. They developed EACLD model taking into account the effects of edge elements. Although the edge element, allowed an increase in the transmissibility between the actuator and the structure, the shear strain in the viscoelastic layer was reduced thus reducing the passive damping in the system. Badre et. al. [9] investigated the feasibility of EACLD on helicopter flex beams for aeromechanical stability augmentation.

Lam et. al. [10] proposed four ACLD configurations separating AD and PCLD treatments bonded on the same side and on the opposite sides of a beam, leading to the so called AD/PCLD treatments. Their theoretical results showed that, for the case studied, the AD/PCLD treatments were more effective and require less control voltages than the ACLD, and that AD/PCLDs were more effective when active and passive treatments were placed on opposite sides. Recently, Garg and Anderson [11] reported the advances made in the area of vibration suppression via constrained layer damping treatments.

Several theoretical studies have indicated the effectiveness of ACLD treatments, compared to purely active and purely passive damping treatments. Experimental investigations have, however, been limited. The goal of this research is to conduct systematic theoretical and experimental investigations starting from simple bare-beam to the beam partially covered with ACLD treatment. A cantilever beam has been used as a base structure. In all, four systems have been studied viz., bare beam, beam-piezo (AD), beam-VEM (PCLD), and beam-VEM-piezo (ACLD). A beam finite element (FE) model has been formulated with ACLD on both sides of beam, incorporat-

ing the effect of shear deformation in the VEM. The VEM layer is modeled using Golla-Hughes-McTavish (GHM) method [12, 13]. The effect of a passive aluminum constraining layer is also incorporated into the beam FE model. Theoretical predictions of dynamic behavior obtained using FE model have been shown to match very well with experimental observations.

Finite Element Formulation

As shown in Fig.1, a uniform thickness cantilever beam partially covered with ACLD , treatment is considered. A linear, Euler-Bernoulli theory based beam finite element model as developed in references [8, 9] is extended for ACLD on both sides of beam. The effect of passive aluminum constraining layer is included. The same ACLD treatments are assumed to be on both sides of the beam. Two types of elements are considered (1) Beam elements with ACLD treatment (2) Plain Beam elements. Plain beam elements are standard and formulation of beam elements with ACLD treatment is described below.

Beam Elements with ACLD Treatment

Kinematic Relationships

The deformation of the generic element is as shown in Fig.2. The axial displacement of the centre line of the active piezoelectric constraining layer, passive aluminum constraining layer, the viscoelastic shear layer and the beam are u_p, u_a, u_v, and u_b, respectively. Here, w denotes the transverse displacement. The subscripts *le* and *te* refer to the leading edge and trailing edge of the beam, respectively.

From Fig.2, the shear strain γ of the VEM is given by

$$\gamma_{le,\,te} = \frac{\partial w}{\partial x} - \psi_{le,\,te} \tag{1}$$

where ψ is the rotational angle of the VEM layer. Assuming perfect bonding conditions, the following kinematic relations can be derived.

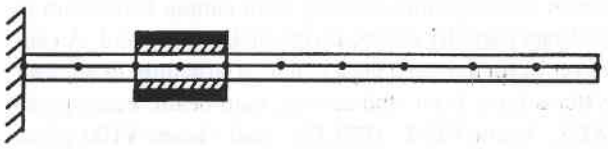

Fig. 1 Typical beam element model of a cantilever beam partially covered with ACLD

$$u_{vle,\,te} = u_b \mp \frac{t_b}{2}\frac{\partial w}{\partial x} - \frac{t_v}{2}\psi_{le,\,te}$$

$$= u_b \mp \frac{t_b + t_v}{2}\frac{\partial w}{\partial x} + \frac{t_v}{2}\gamma_{le,\,te} \tag{2}$$

$$u_{ale,\,te} = u_b \mp \frac{t_b + t_a}{2}\frac{\partial w}{\partial x} - t_v\,\psi_{le,\,te}$$

$$= u_b \mp \left[\frac{t_b + t_a}{2} + t_v\right]\frac{\partial w}{\partial x} - t_v(-\gamma_{le,\,te})$$

$$= u_b \mp r\frac{\partial w}{\partial x} + t_v\gamma_{le,\,te} \tag{3}$$

$$u_{ple,\,te} = u_b \mp \left(\frac{t_b + t_p}{2} + t_a\right)\frac{\partial w}{\partial x} - t_v\,\psi_{le,\,te}$$

$$= u_b \mp \left[\frac{t_b + t_p}{2} + t_a + t_v\right]\frac{\partial w}{\partial x} - t_v(-\gamma_{le,\,te})$$

$$= u_b \mp h\frac{\partial w}{\partial x} + t_v\gamma_{le,\,te} \tag{4}$$

where $r = t_v + \frac{t_b + t_a}{2}$, $h = t_v + t_a + \frac{t_b + t_p}{2}$

Shape Functions

The transverse displacement w is interpolated using standard cubic polynomial in x defined over the element length L_e. The axial displacement u_b and shear angle γ are interpolated using standard linear polynomial in x defined over the element length L_e. The nodal d.o.f. for the ACLD elements (Fig.3) are given by

$$\{q\}_e = \left[w_1\ w_1'\ u_1\ \gamma_1\ w_2\ w_2'\ u_2\ \gamma_2\right]^T \tag{5}$$

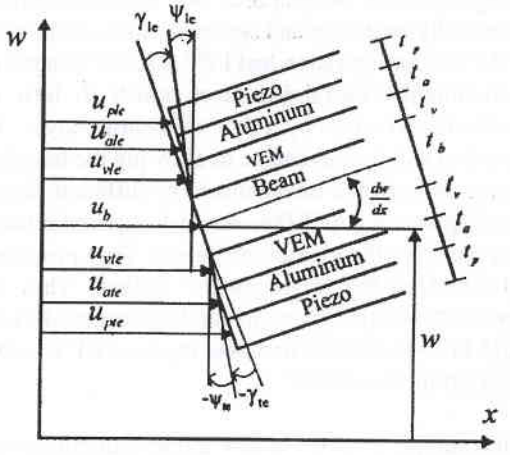

Fig. 2 The deformation of a beam with ACLD

The transverse displacement, axial displacement, and shear angle are expressed in terms of the nodal displacements by finite element shape functions as:

$$w = [N_w(x)]\{q\}_e \; ; \; u_b = [N_u(x)]\{q\}_e \; ; \; \gamma\,[N_\gamma(x)]\{q\}_e \quad (6)$$

where the shape functions are given by,

$$[N_w(x)]^T = \begin{bmatrix} 1-3\left(\frac{x}{L_e}\right)^2+2\left(\frac{x}{L_e}\right)^3 \\ \left[\left(\frac{x}{L_e}\right)-2\left(\frac{x}{L_e}\right)^2+\left(\frac{x}{L_e}\right)^3\right]L_e \\ 0 \\ 0 \\ 3\left(\frac{x}{L_e}\right)^2-2\left(\frac{x}{L_e}\right)^3 \\ \left[-\left(\frac{x}{L_e}\right)^2+\left(\frac{x}{L_e}\right)^3\right]L_e \\ 0 \\ 0 \end{bmatrix}$$

$$[N_u(x)]^T = \left[0\;0\;1-\left(\frac{x}{L_e}\right)\;0\;0\;0\;\left(\frac{x}{L_e}\right)\;0\right]'$$

$$[N_\gamma(x)]^T = \left[0\;0\;0\;1-\left(\frac{x}{L_e}\right)\;0\;0\;0\;\left(\frac{x}{L_e}\right)\right]' \quad (7)$$

Fig. 3 Nodal d.o.f. of ACLD beam element

from Eqs. (2) - (7)

$$u_{vle,\,te} = \left[\mp\frac{t_b+t_b}{2}\;1\;\frac{t_v}{2}\right]\begin{bmatrix}[N_w']\\[N_u]\\[N_\gamma]\end{bmatrix}\{q\} \quad (8)$$

$$u_{ale,\,te} = \left[\mp r\;1\;t_v\right]\begin{bmatrix}[N_w']\\[N_u]\\[N_\gamma]\end{bmatrix}\{q\} \quad (9)$$

$$u_{ple,\,te} = \left[\mp h\;1\;t_v\right]\begin{bmatrix}[N_w']\\[N_u]\\[N_\gamma]\end{bmatrix}\{q\} \quad (10)$$

Modeling of the Base Beam

The potential energy of the beam in bending is

$$\frac{1}{2}E_b I_b\int_0^{L_e}\left(\frac{\partial^2 w}{\partial x^2}\right)^2 dx = \frac{1}{2}\{q\}^T\left[K_{wb}^{(e)}\right]\{q\},$$

$$\text{where } [K_{wb}] = E_b I_b\int_0^{L_e}\left[N_w''\right]^T\left[N_w''\right]\,dx \quad (11)$$

The potential energy of the beam due to extension is

$$\frac{1}{2}E_b A_b\int_0^{L_e}\left(\frac{\partial u_b}{\partial x}\right)^2 dx = \frac{1}{2}\{q\}^T\left[K_{ub}\right]\{q\},$$

$$\text{where } [K_{ub}] = E_b A_b\int_0^{L_e}\left[N_u'\right]^T\left[N_u'\right]\,dx \quad (12)$$

The kinetic energy of the beam associated with transverse motion is

$$\frac{1}{2}\rho_b A_b\int_0^{L_e}\left(\frac{\partial w}{\partial t}\right)^2 dx = \frac{1}{2}\{\dot{q}\}^T\left[M_{wb}\right]\{\dot{q}\},$$

$$\text{where } [M_{wb}] = \rho_b A_b\int_0^{L_e}\left[N_w\right]^T\left[N_w\right]\,dx \quad (13)$$

The kinetic energy of the beam associated with axial motion is

$$\frac{1}{2}\rho_b A_b \int_0^{L_e}\left(\frac{\partial u_b}{\partial t}\right)^2 dx = \frac{1}{2}\{\dot{q}\}^T\left[M_{ub}\right]\{\dot{q}\},$$

$$\text{where } [M_{ub}] = \rho_b A_b \int_0^{L_e}\left[N_u\right]^T\left[N_u\right] dx \qquad (14)$$

Modeling of the Aluminum (Passive) Constraining Layer

The potential energy of the aluminum layer due to bending is given by

$$\frac{1}{2}E_a I_a \int_0^{L_e}\left(\frac{\partial^2 w}{\partial x^2}\right)^2 dx = \frac{1}{2}\{q\}^T\left[K_{wa}^{(e)}\right]\{q\},$$

$$\text{where } [K_{wa}] = E_a I_a \int_0^{L_e}\left[N_w''\right]^T\left[N_w''\right] dx \qquad (15)$$

where I_a is the second moment of area of aluminum layer as referred to the neural axis of the system.

The potential energy of the aluminum layer due to extension is

$$\frac{1}{2}E_a I_a \int_0^{L_e}\left(\left(\frac{\partial u_{ale}}{\partial x}\right)^2 + \left(\frac{\partial u_{ate}}{\partial x}\right)^2\right) dx = \frac{1}{2}\{q\}^T[K_{ua}]\{q\}$$

where

$$[K_{ua}] = E_a A_a \int_0^{L_e}\begin{bmatrix}[N_w'']\\ [N_u']\\ [N_\gamma']\end{bmatrix}^T\begin{Bmatrix}-r\\ 1\\ t_v\end{Bmatrix}\begin{Bmatrix}-r & 1 & t_v\end{Bmatrix}\begin{bmatrix}[N_w'']\\ [N_u']\\ [N_\gamma']\end{bmatrix}$$

$$+\begin{bmatrix}[N_w'']\\ [N_u']\\ [N_\gamma']\end{bmatrix}^T\begin{Bmatrix}r\\ 1\\ t_v\end{Bmatrix}\begin{Bmatrix}r & 1 & t_v\end{Bmatrix}\begin{bmatrix}[N_w'']\\ [N_u']\\ [N_\gamma']\end{bmatrix} dx \qquad (16)$$

The kinetic energy of the aluminum layer associated with transverse motion is

$$2\left\{\frac{1}{2}\rho_a A_a \int_0^{L_e}\left(\frac{\partial w}{\partial t}\right)^2 dx\right\} = \frac{1}{2}\{\dot{q}\}^T[M_{wa}]\{\dot{q}\},$$

$$\text{where } [M_{wa}] = 2\rho_a A_a \int_0^{L_e}[N_w]^T[N_w] dx \qquad (17)$$

Note that the factor '2' in multiplied since both sides of the beam are treated with ACLD. This is applicable for the piezoelectric and VEM layers also.

The kinetic energy of the aluminum layer associated with axial motion is

$$\frac{1}{2}\rho_a I_a \int_0^{L_e}\left(\left(\frac{\partial u_{ale}}{\partial t}\right)^2 + \left(\frac{\partial u_{ate}}{\partial t}\right)^2\right) dx = \frac{1}{2}\{\dot{q}\}^T[M_{ua}]\{\dot{q}\}$$

where

$$[M_{ua}] = \rho_a A_a \int_0^{L_e}\begin{bmatrix}[N_w']\\ [N_u]\\ [N_\gamma]\end{bmatrix}^T\begin{Bmatrix}-r\\ 1\\ t_v\end{Bmatrix}\begin{Bmatrix}-r & 1 & t_v\end{Bmatrix}\begin{bmatrix}[N_w']\\ [N_u]\\ [N_\gamma]\end{bmatrix}$$

$$+\begin{bmatrix}[N_w']\\ [N_u]\\ [N_\gamma]\end{bmatrix}^T\begin{Bmatrix}r\\ 1\\ t_v\end{Bmatrix}\begin{Bmatrix}r & 1 & t_v\end{Bmatrix}\begin{bmatrix}[N_w']\\ [N_u]\\ [N_\gamma]\end{bmatrix} dx \qquad (18)$$

Modeling of the Piezoelectric Active Constraining (Actuator) Layer

The potential energy of the piezoelectric layer due to bending is given by

$$\frac{1}{2}E_p I_p \int_0^{L_e}\left(\frac{\partial^2 w}{\partial x^2}\right)^2 dx = \frac{1}{2}\{q\}^T\left[K_{wp}^{(e)}\right]\{q\},$$

$$\text{where } [K_{wp}] = E_p I_p \int_0^{L_e}\left[N_w''\right]^T\left[N_w''\right] dx \qquad (19)$$

where I_p is the second moment of area of piezoelectric layer as referred to the neutral axis of the system.

The potential energy of the piezoelectric layer due to extension is

$$\frac{1}{2}E_p A_p \int_0^{L_e}\left(\left(\frac{\partial u_{ple}}{\partial x}\right)^2 + \left(\frac{\partial u_{pte}}{\partial x}\right)^2\right) dx = \frac{1}{2}\{q\}^T[K_{up}]\{q\}$$

where

$$[K_{up}] = E_p A_p \int_0^{L_e} \begin{bmatrix} [N_w''] \\ [N_u'] \\ [N_\gamma'] \end{bmatrix}^T \begin{Bmatrix} -h \\ 1 \\ t_v \end{Bmatrix} \{-h \quad 1 \quad t_v\} \begin{bmatrix} [N_w''] \\ [N_u'] \\ [N_\gamma'] \end{bmatrix}$$

$$+ \begin{bmatrix} [N_w''] \\ [N_u'] \\ [N_\gamma'] \end{bmatrix}^T \begin{Bmatrix} h \\ 1 \\ t_v \end{Bmatrix} \{h \quad 1 \quad t_v\} \begin{bmatrix} [N_w''] \\ [N_u'] \\ [N_\gamma'] \end{bmatrix} dx \qquad (20)$$

The kinetic energy of the piezoelectric layer associated with transverse motion is

$$2\left\{\frac{1}{2}\rho_p A_p \int_0^{L_e} \left(\frac{\partial w}{\partial t}\right)^2 dx\right\} = \frac{1}{2}\{\dot{q}\}^T [M_{wp}] \{\dot{q}\},$$

$$\text{where } [M_{wp}] = 2\rho_p A_p \int_0^{L_e} [N_w]^T [N_w]\, dx \qquad (21)$$

The kinetic energy of the piezoelectric layer associated with axial motion is

$$\frac{1}{2}\rho_p A_p \int_0^{L_e} \left(\left(\frac{\partial u_{ple}}{\partial t}\right)^2 + \left(\frac{\partial u_{pte}}{\partial t}\right)^2\right) dx = \frac{1}{2}\{\dot{q}\}^T [M_{up}] \{\dot{q}\}$$

where

$$[M_{up}] = \rho_p A_p \int_0^{L_e} \begin{bmatrix} [N_w'] \\ [N_u] \\ [N_\gamma] \end{bmatrix}^T \begin{Bmatrix} -h \\ 1 \\ t_v \end{Bmatrix} \{-h \quad 1 \quad t_v\} \begin{bmatrix} [N_w'] \\ [N_u] \\ [N_\gamma] \end{bmatrix}$$

$$+ \begin{bmatrix} [N_w'] \\ [N_u] \\ [N_\gamma] \end{bmatrix}^T \begin{Bmatrix} h \\ 1 \\ t_v \end{Bmatrix} \{h \quad 1 \quad t_v\} \begin{bmatrix} [N_w'] \\ [N_u] \\ [N_\gamma] \end{bmatrix} dx \qquad (22)$$

The virtual work done by the induced strain (force) in the piezoelectric patch under the applied voltage $V(t)$

$$\int_0^{L_e} E_p d_{31} bV(t)\, \delta\left(\frac{\partial u_p}{\partial x}\right) dx$$

$$= E_p d_{31} bV(t) \left(\delta u_p \Big|_{x=L_e} - \delta u_p \Big|_{x=0}\right)$$

$$E_p d_{31} bV(t) \{\delta q\}_e^T \left(\begin{bmatrix} N_w'(L_e) \end{bmatrix} \begin{Bmatrix} -h \\ 1 \\ t_v \end{Bmatrix} \begin{bmatrix} [N_w'(0)] \\ [N_u(0)] \\ [N_\gamma(0)] \end{bmatrix} \begin{Bmatrix} -h \\ 1 \\ t_v \end{Bmatrix} \right)$$

$$= \{\delta q\}_e^T E_p d_{31} bV(t) \times \{0 \quad h \quad -1 \quad -t_v \quad 0 \quad -h \quad 1 \quad t_v\}^T$$

$$= \{\delta q\}_e^T \{P_c\}_e V(t) \qquad (23)$$

Modeling of the VEM (Shear) Layer

Golla-Hughes-McTavish (GHM) method [12, 13] is employed to analyse the Stieltjes integral in time domain [8]. The GHM method represents the material modulus function as a series of mini-oscillator terms in Laplace domain [14].

$$s\tilde{G}(x) = G_0 \left(1 + \sum_{n=1}^{k} \hat{\alpha}_n \frac{s^2 + 2\hat{\zeta}_n \hat{\omega}_n s}{s^2 + 2\hat{\zeta}_n \hat{\omega}_n s + \hat{\omega}_n^2}\right)$$

$$= G_0 (1 + h(s)) \qquad (24)$$

where, the leading factor G_o is the equilibrium value of the modulus, i.e. the final value of the relaxation function $G(t)$. The GHM parameters G_o and α can be related to the shear modulus and loss factor of VEMs. From a single-term GHM expression, the following time-domain pair of equations can be obtained.

$$G_\gamma = (G_0 + \alpha G_0)_\gamma - \alpha G_0 z \qquad (25)$$

$$\left(\alpha G_0 \frac{1}{\hat{\omega}^2}\right)\ddot{z} + \left(\alpha G_0 \frac{2\hat{\zeta}}{\hat{\omega}}\right)\dot{z} - \alpha G_0 \gamma + \alpha G_0 z = 0 \qquad (26)$$

where z is the dissipation coordinate which may be expressed as follows:

$$z = N_z(x)\{z\} = \begin{bmatrix} 1 - \frac{x}{L_e} & \frac{x}{L_e} \end{bmatrix} \begin{Bmatrix} z_1 \\ z_2 \end{Bmatrix} \tag{27}$$

The virtual work done by the viscoelastic layer is therefore

$$-A_v \int_0^{L_e} (G\gamma)\,\delta\gamma\,dx = -A_v \{\delta q\}_e^T \int_0^{L_e} [N_\gamma]^T (G\gamma)\,dx$$

$$= -A_v \{\delta q\}_e^T ((G_0 + \alpha G_0) \int_0^{L_e} [N_\gamma]^T [N_\gamma]\,dx \{q\}_e$$

$$- \alpha G_0 \int_0^{L_e} [N_\gamma]^T [N_z]\,dx \{z\})$$

$$= -\{\delta q\}_e^T [K_v] \{q\}_e + \{\delta q\}_e^T [K_{qz}] \{z\} \tag{28}$$

where

$$[K_v] = A_v G_0 (1+\alpha) \int_0^{L_e} [N_\gamma]^T [N_\gamma]\,dx \tag{29}$$

$$[K_{qz}] = A_v \alpha G_0 \int_0^{L_e} [N_\gamma]^T [N_z]\,dx \tag{30}$$

From Eq. (26),

$$[M_z]\{\ddot{z}\} + C_z\{\dot{z}\} - [K_{zq}]\{q\}_e + [K_z]\{z\} = 0 \tag{31}$$

where

$$[K_{zq}] = A_v \alpha G_0 \int_0^{L_e} [N_z]^T [N_\gamma]\,dx = [K_{qz}]^T \tag{32}$$

$$[K_z] = A_v \alpha G_0 \int_0^{L_e} [N_z]^T [N_z]\,dx \tag{33}$$

$$[M_z] = A_v \alpha G_0 \frac{1}{\hat{\omega}^2} \int_0^{L_e} [N_z]^T [N_z]\,dx \tag{34}$$

$$[C_z] = A_v \alpha G_0 \frac{2\hat{\zeta}}{\hat{\omega}^2} \int_0^{L_e} [N_z]^T [N_z]\,dx \tag{35}$$

Mass, Damping, and Stiffness Matrices of ACLD Elements

The final mass, damping, and stiffness Matrices for single ACLD element can be expressed in the following form:

$$[M_e] = [M_{wb}] + [M_{wa}] + [M_{wp}] + [M_{wv}] + [M_{ub}]$$

$$+ [M_{ua}] + [M_{up}] + [M_{uv}] \tag{36}$$

$$[K_e] = [K_{wb}] + [K_{wa}] + [K_{wp}] + [K_{ub}] + [K_{ua}]$$

$$+ [K_{up}] + [K_v] \tag{37}$$

The matrices corresponding to $\{q\}$ and $\{z\}$ are $[K_{qz}]$ and $[K_{zq}]$. The matrices corresponding to $\{z\}$ are $[M_z]$, $[C_z]$, and $[K_z]$.

Equations of Motion of the Beam Partially Covered with ACLD Treatment

Using Hamilton's principle, the final equations of motion for an element are obtained as,

$$\begin{bmatrix} [M]_e & [0] \\ [0] & [M_z] \end{bmatrix} \begin{Bmatrix} \{\ddot{q}\}_e \\ \{\ddot{z}\}_e \end{Bmatrix} + \begin{bmatrix} [0] & 0 \\ 0 & [C_z] \end{bmatrix} \begin{Bmatrix} \{\dot{q}\}_e \\ \{\dot{z}\}_e \end{Bmatrix}$$

$$+ \begin{bmatrix} [K]_e & -[K_{qz}] \\ -[K_{zq}] & [K_z] \end{bmatrix} \begin{Bmatrix} \{q\}_e \\ \{z\}_e \end{Bmatrix} = \begin{Bmatrix} \{P_c\}_e \{V(t)\}_e + \{f_d\}_e \\ \{0\} \end{Bmatrix} \tag{38}$$

It is observed that the size of the element matrices is (6 x 6) for a plain beam element; (8 x 8) for a beam element with ACLD treatment and these two types of elements are joined together through a standard transition element of size(7x7). The elemental dissipation coordinates $\{z_e\}$ are considered as additional nodal degrees-of-freedom. The global equations of motion can be obtained by assembling the elemental equations and are given by

$$[M]\{\ddot{q}\} + [C]\{\dot{q}\} + [K]\{q\} = \{F\} \tag{39}$$

where $\{q\}$, $\{\dot{q}\}$ and $\{\ddot{q}\}$ are the global displacement, velocity and acceleration vectors, respectively (including GHM dissipation coordinates), [M], [C] and [K] are the mass, damping and stiffness matrices. $\{P_c\}$ is the piezoelectric force vector which maps the applied voltage to the induced displacements and $\{f_d\}$is the vector representing external disturbance forces if any. Equation (23) is used for calculating $\{f_d\}$ also, since piezoelectric exciter patch is used for exciting the system and no other external forces are considered. The discretized Eq.(39) is cast in state-space form and numerical simulations are carried out in MATLAB®6.1 (R12.1). To validate the FE model for the

beam partially covered with ACLD treatment, a set of experiments are conducted.

Piezoelectric Actuator Placement

The actuators should be placed at the locations to excite the desired modes most effectively. The piezoelectric actuators should be placed in regions of high average strain and away from areas of zero strain. The location of these 'strain nodes' are determined by twice differentiating the mode shape functions of a bare cantilever beam and finding the zero-crossing points of the resulting functions [15]. The piezoelectric actuator's (PZTs) must be placed away from strain nodes, so that the strain applied over the entire length of the actuator has a constant phase with respect to the homogenous strain in the beam with corresponding mode. If not, modal force produced, by the actuator will be decreased, since one section of the actuator will be opposing the other. All flexible structures will have number of strain nodes in all their elastic modes. Therefore, in order to control the flexural modes effectively, it is necessary to control independently the driving voltage applied to each PZT. This cannot be done if the actuator is continuous over the length of the beam. Analytical mode-shapes for the bare beam (unit length) are shown in the Fig.4. The first four transverse bending mode-shapes predicted using FEM are found to be matching (Fig.4) with the analytical mode-shapes.

In this analysis, a bare-beam of unit length is considered first and different strain nodes up to the first four modes are found. The first four modes together have six strain nodes and seven regions (Table-1) where piezoelectric actuator could be placed (Fig.5). With this analysis, there is choice for selecting either length of piezoelectric actuator or beam. Table-2 shows different alternatives for piezoelectric patch placement by fixing the patch length (say 40 mm). It is observed that alternatives (1, 2 and 3) are not suitable for desired purpose due to longer beam lengths leading to possible large deflection problems. A piezoelectric patch placed more towards the tip may not be effective in exciting higher modes [16]. Alternatives 5-7 suffer from this disadvantage and hence alternative-4 has been selected.

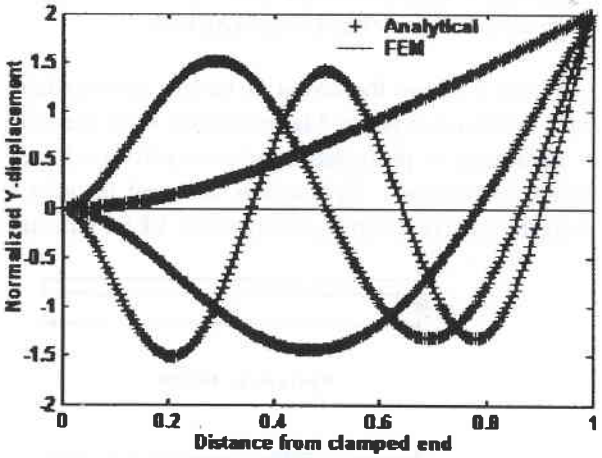

Fig. 4 Comparison of finite element and analytically predicted mode-shapes

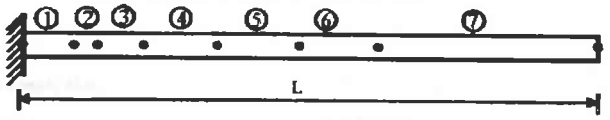

Fig.5 Locations of piezoelectric patch along the length of beam

Table -1 : Regions for piezoelectric actuator placement

Region	Piezoelectric patch length (mm)	Distance from the fixed end (mm)
1	0.0952 L	0.0
2	0.0315 L	0.0952 L
3	0.0902 L	0.1267 L
4	0.1413 L	0.2169 L
5	0.1418 L	0.3582 L
6	0.1393 L	0.5 L
7	0.3601 L	0.6393 L

Table -2 : Alternatives for piezoelectric actuator placement

Alternative	Length of piezoelectric patch (mm)	Beam length (mm)	Distance from the fixed end (mm)
1	0.0952 L	420.16	0
2	0.0315 L	1269.84	120.88
3	0.0902 L	443.45	56.18
4	0.1413 L	283.08	61.40
5	0.1418 L	282.08	101.04
6	0.1393 L	287.15	143.57
7	0.3601 L	111.08	71.01

Experimental Validation

A cantilever beam is used as the base structure. In all, four systems have been fabricated and tested. Beams of required dimensions are cut from a single sheet of aluminum. The various systems studied include:

System 1: Beam
System 2: Beam-Piezo (AD)
System 3: Beam-VEM (PCLD)
System 4: Beam- VEM-Piezo (ACLD)

Figure 6 shows the layout of various systems fabricated and tested. System-2 is analyzed to study the effect of application of piezoelectric actuator patch on the dynamics of System-1. System-3 is analyzed in order to study the passive damping ability of the VEM, reduction in resonance amplitude and settling time for a given disturbance. Commercially available VEM damping polymer 3M ISD 112 with the backing of aluminum passive constraining layer is used as a damping layer. In System-4, commercially available piezoelectric patches (SP-5H) are used as active constraining layers in addition to the VEM damping polymers 3M ISD 112 as passive damping layers. Mainly, the combined effects of the VEM and piezoelectric patch on passive damping ability and active action transmissibility are studied in System-4.

The properties of beam, VEM damping polymer and piezoelectric actuator are listed in Table-3. The properties like density, modulus of elasticity, and structural damping of the beam are determined by simple experiments. Young's modulus of elasticity is found based on the experimental value of the fundamental frequency and

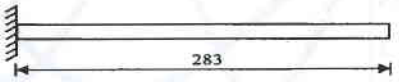

System 1: Beam

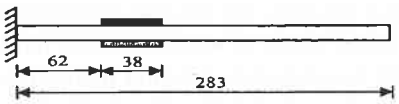

System 2: Beam-Piezo (AD)

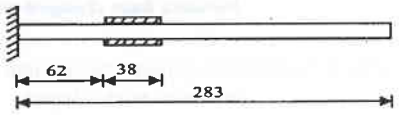

System 3: Beam-VEM (PCLD)

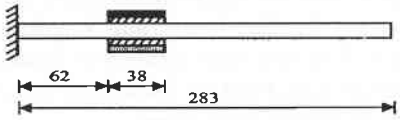

System 4: Beam-VEM-Piezo (ACLD)

All dimensions are in mm

Beam | VEM with aluminum constraining layer
Piezoelectric control actuator | Piezoelectric disturbance exciter

Fig. 6 Layout of different systems investigated

Table -3 : Properties of beam specimen, VEM damping polymer and piezoelectric actuator

Property	Beam	Viscoelastic**	Constraining layer	Piezoelectric actuator
Material	Aluminum	3M ISD 112***	Aluminum	SP-5H****
Cross Section (mm)	25 x 0.439	25 x 0.127	25 x 0.0508	25 x 0.35
Density (kg/m^3)	2400.43*	1600	2700	7500
Modulus of Elasticity (N/m^2)	59.28×10^9*	0.01×10^9	70×10^9	62×10^9

* Experimentally determined

** The values quoted corresponding to shear modulus of ISD 112 and Young's modulus for the other materials

*** ISD 112 is a commercial viscoelastic manufactured by the 3M company (http://www.3m.com) available as a CLD preparation including the aluminium constraining layer and loss factor (0.5 - 1.1)

**** SP-5H is manufactured by Sparkler Ceramics Pvt Ltd, India (http://www.sparklerceramics.com) with $d_{31} = -247 \times 10^{-12}$ m/V

using the theoretical formula for the fundamental frequency of a cantilever beam in bending. The structural damping factor is determined by the free vibration response using logarithmic decrement.

Natural Frequency Studies

System-1 and System-3 are excited manually while piezoelectric actuators (SP-5H) are used for exciting System-2 and System-4 in different modes. Fig.7 shows the photograph of the System-2 with the non-contact Fiber Optic (FO) displacement sensor in position. The schematic of the experimental setup is shown in Fig.8. A sweep function generator (APLAB, Model FG2M) which generates signals of variable frequency is used as a signal source. A sinusoidal signal from this sweep function generator is fed to the piezo amplifier (TREK, Model PZD350) for signal amplification which in turn is given to the piezoelectric exciter for exciting the system. The corresponding tip deflection response is measured using the non-contact FO displacement sensor probe (PHILTEC, Model D169) which is located very near the free end of the system. The output of FO sensor is given to an oscilloscope (TEKTRONIX, Model TDS210) where it is processed through its FFT module. Theoretical and experimental natural frequencies for the first five modes of all the systems are studied.

The first five natural frequencies as predicted by FEM are compared with experiments for Systems-1 to 4 in Table-4. It is observed that FEM and experimental values are matching very well (worst error less than 6%). For the systems studied here, theoretical predictions (Table-4) indicate that the fundamental frequency is increased by the addition of the VEM and/or piezoelectric layers. This is corroborated by experimental observations. Similarly frequencies of modes 2-5 are predicted to be lower for Systems-2 and 4 compared to System-1 and are again corroborated by experimental observations. Interestingly, frequencies of modes 2-5 are predicted to be increased for System-3 as compared to System-1 while it is experimentally observed that these are somewhat reduced.

Free Vibration Response Studies

The open loop free vibration response due to an initial disturbance (viz., displacing the tip of the beam by a fixed distance of 5 mm) of various systems is studied. The open loop experiments are performed on all systems using a real time data acquisition and software controller, dSPACE®3.2 - ControlDesk®2.2. The signal from the

Table - 4: Comparison of experimental and FEM natural-frequencies (Hz)

Mode	System	FEM	Experimental
1	1	4.40	4.38
	2	4.71	4.58
	3	4.66	4.50
	4	4.73	4.68
2	1	27.57	28.00
	2	22.52	22.00
	3	27.93	27.00
	4	22.01	21.00
3	1	77.21	76.60
	2	67.90	67.50
	3	80.15	75.50
	4	68.36	65.00
4	1	151.30	156.00
	2	142.89	139.50
	3	155.37	145.60
	4	142.32	140.10
5	1	250.12	255.00
	2	233.39	230.00
	3	253.42	249.75
	4	231.89	230.00

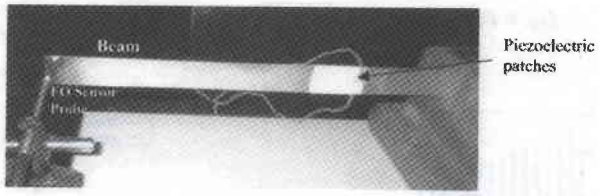

Fig.7 Photograph of the beam with piezoelectric patches

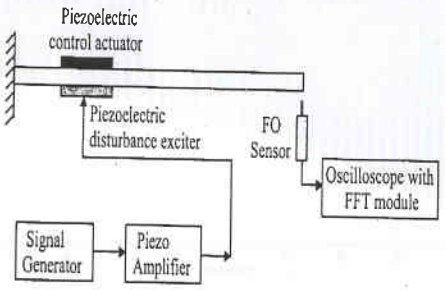

Fig.8 Schematic of the open loop experimental set-up

system (FO sensor output) is converted to a digital signal in the ADC on the hardware part of dSPACE®. ControlDesk® offers the basic environment for all the elements and tools offered by dSPACE®. The signal characteristics are studied using ControlDesk®. Damping ratio and settling time are studied for all the systems.

The theoretical and experimental tip responses (when the tip of the system is displaced by a fixed distance of 5 mm and released) measured for the first 10 seconds for Systems-1 to 4 are shown in Figs.9-12, respectively. It is observed that, in all cases, the finite element and experimental results are matching very well. When the VEM and piezoelectric layer are bonded to the beam, while enhancing the damping, they change the mass/stiffness properties also. The net effect on natural frequency will depend on the relative axial location of VEM/piezoelectric layer with respect to the mode shape. It is observed that the value of damping ratio increases monotonically while the settling time (the time required for the response of a system to reach within a band of 2% of initial displacement) decreases monotonically from System-1 to System-4. The application of the VEM (System-3) offers significant amount of passive damping (145% increase in damping ratio as compared to System-1) as compared to addition of the piezoelectric patch as in System-2 (23% increase in damping ratio as compared to System-1).

System-4 is found to be better (215% increase in damping ratio compared to System-1) than System-2 and 3 as the passive vibrations settle quickly (71 % reduction in settling time when compared to System-1). The values

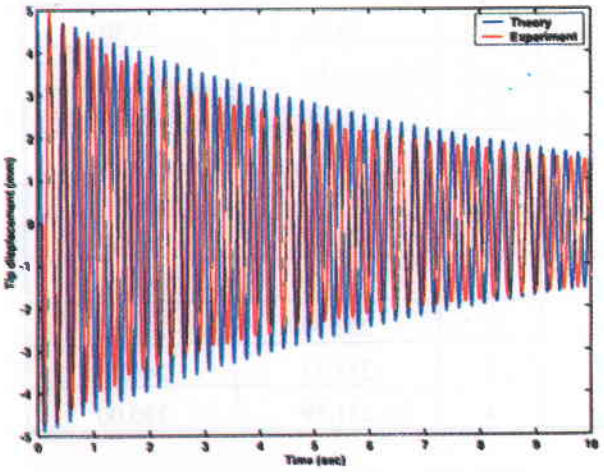

Fig. 9 Free vibration response at the tip (System-1)

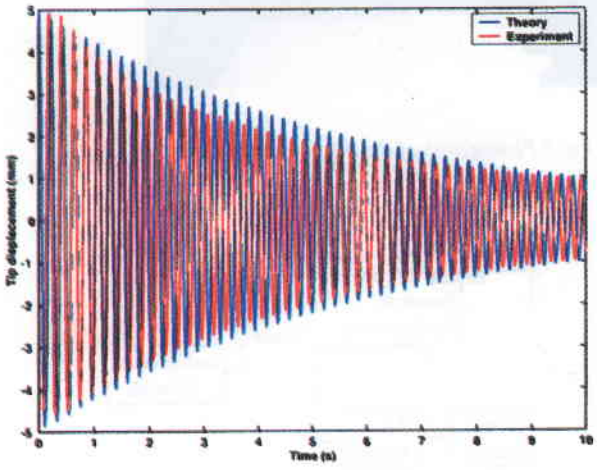

Fig. 10 Free vibration response at the tip (System-2)

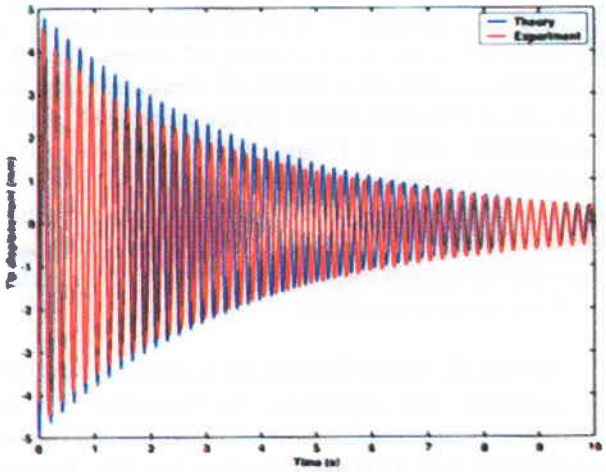

Fig. 11 Free vibration response at the tip (System-3)

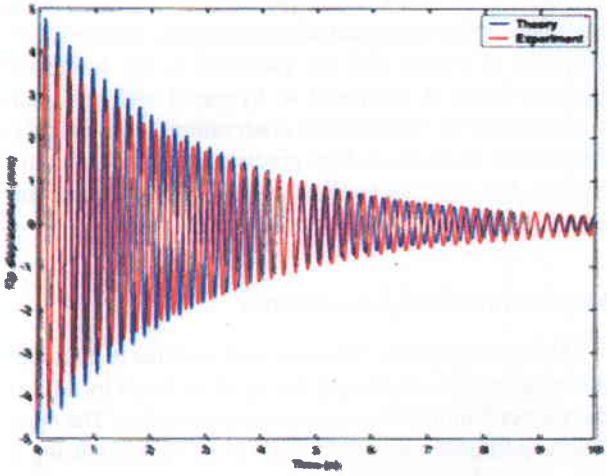

Fig. 12 Free vibration response at the tip (System-4)

of damping ratios and settling times for all the systems investigated are compared in Table-5. VEM and ACLD treatments, while enhancing the damping, contribute to the system stiffness/inertia also. The frequencies of the system may be designed to lie in a particular range vis-a-vis the operating frequencies and so it is important that the provision of additional damping through these does not change the system frequencies drastically. The percentage change in fundamental frequency is also given in Table-5.

Table - 5: Comparison of damping ratio and settling time for various systems

System	Damping Ratio	Settling Time (s)	% Change in Fundamental Frequency w.r.t. System-1
1	0.0035	41.52	--
2	0.0043	32.94	4.56
3	0.0086	16.45	2.73
4	0.0110	12.36	6.84

Active Control of Forced Vibration Response

The effect of application of control on forced vibration response is now studied. Two piezoelectric patches are used, one acting as the control actuator and the other as the disturbance exciter. The theoretically predicted and experimentally observed tip deflection responses of Systems-2 and 4 when the piezoelectric disturbance exciter patch is subjected to sinusoidal voltage of V_o sin ($\omega_1 t$) (where $V_o = \pm 50$V and ω_1 = first natural frequency of the respective systems) are now compared. A set of experiments are performed with Direct Velocity Feedback (DVF) control strategy. Different values of gains are implemented experimentally to study the effect of DVF control on the dynamics of various systems. A non-contact Fiber-Optic (FO) displacement sensor located at the tip of the system is used as a feedback sensor. Two parameters are used for comparative study of various systems with respect to System-2 viz., the resonant amplitude of vibration before the feedback controller is switched on and the stabilized amplitude of vibration after the controller is turned on. As a measure of the control effort expended in achieving the reduction in vibration amplitude, the peak

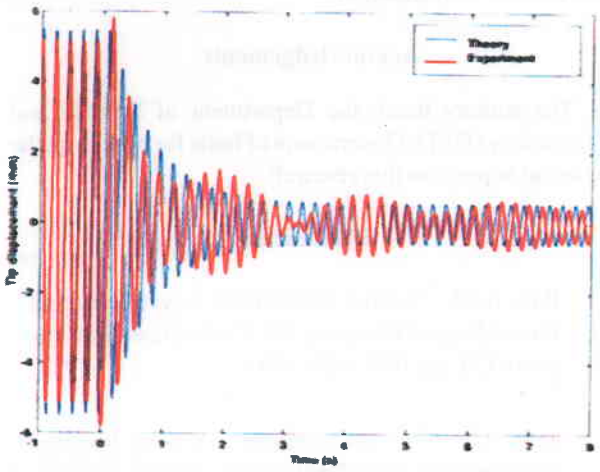

Fig. 13 Tip displacement in forced vibration (system-2) before and after control (k_{dvf} = -1.5)

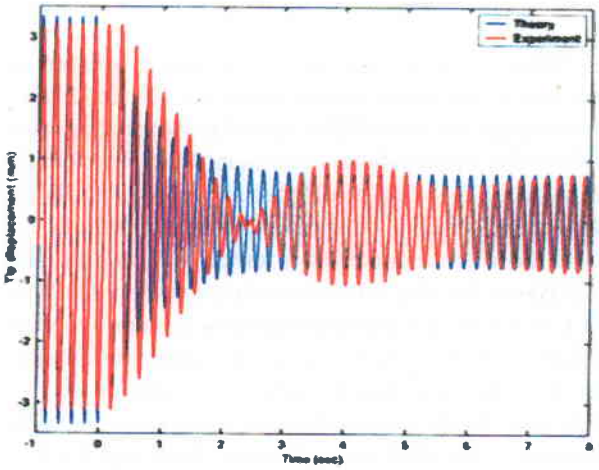

Fig. 14 Tip displacement in forced vibration (system-4) before and after control(k_{dvf} = -1.5)

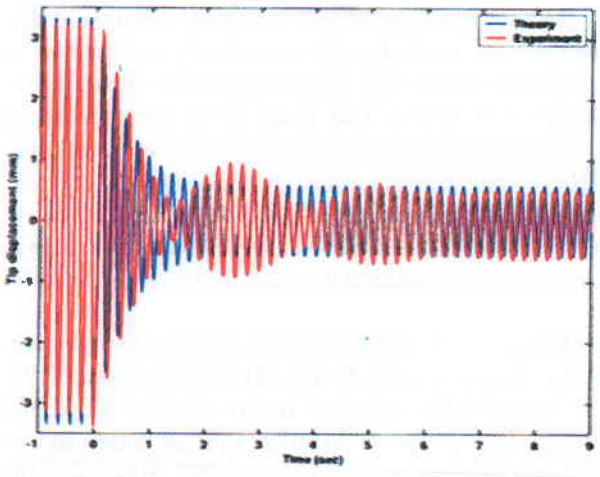

Fig. 15 Tip displacement in forced vibration (system-4) before and after control (k_{dvf} = -2)

Table - 6 : Comparative performance of AD and ACLD systems

Gain k_{dvf}	System	Tip displacement at resonance (mm)			Peak control voltage (V) after stabilization
		Before control	After control	% reduction	
-1.0	2	± 5	± 0.9	82	± 46
	4	± 3.1	± 1.0	67	± 56
-1.5	2	± 5	± 0.625	88	± 46
	4	± 3.1	± 0.75	75	± 56
-2.0	4	± 3.1	± 0.45	85	± 58

voltage on piezoelectric control actuator (after stabilization) is also compared for the various systems.

Figure 13 shows very good comparison between the theoretical and experimental results for System-2, for a few seconds before and after control is switched on. Time $t = 0$ on the x-axis indicates the instant when the controller is switched on. With pure AD treatment (System-2) and k_{dvf} = -1.5, around 88% reduction in tip deflection is achieved after the controller is turned on. However, pure AD system has very little inherent passive damping. A set of experiments are then performed on System-4 to study the effect of the reduction in active control transmissibility from the piezoelectric control actuator to the base structure and the increase in passive damping due to the addition of the VEM to the structure. From Figs.14-15, it is observed that the finite element and experimental results for closed loop active vibration controlled response of the ACLD match very well.

As shown in Figs.14 and 15, the tip vibration amplitude at resonance before the controller is switched on, is reduced by around 38% when compared to vibration amplitude of System-2. This is due to the presence of the VEM damping layers which provide the passive damping. Also the piezoelectric active constraining layers tend to augment the relative in-plane displacements in order to increase the relative shear in the viscoelastic core. This is a very desirable feature as it renders the System-4 fail-safe.

For k_{dvf} = -1.5, System-4 offers around 75% reduction in tip vibration amplitude (Fig.14) whereas System-2 offers around 88% reduction in tip vibration amplitude (Fig.13) after control. With further increase in the value of DVF control gain (k_{dvf} = -2), around 85% reduction in tip vibration amplitude (Fig.15) is observed for System-4 thus approaching the performance of System-2 for k_{dvf} = -1.5.

However, the peak control voltage after stabilization drawn in System-4 is found to be higher (around 22% increase when k_{dvf} = -1.5) than for System-2 (Table-6). It is observed that this voltage increases with increase in DVF control gain in order to achieve the performance of System-2. This clearly indicates that the introduction of the VEM between the piezoelectric actuator and the structure reduces the active control transmissibility from the piezoelectric control actuator patch to the base structure.

Conclusion

A beam finite element model has been developed with Golla-Hughes-McTavish (GHM) method for the frequency dependant behavior of the VEM. Piezoelectric control actuator location is selected based on its control actuation authority (as indicated by regions of high average strain). A very good match between theoretical and experimental predictions has been established for the free vibration transient response as well as closed loop active vibration control situation.

Acknowledgements

The authors thank the Department of Science and Technology (DST), Government of India for providing the financial support to this research.

References

1. Baz, A.M., "Active Constrained Layer Damping", Proceeding of Damping 93, Conference, San Francisco, CA, pp.IBB 1-23, 1993.

2. Shen, I.Y., "Hybrid Damping Through Intelligent Constrained Layer Treatments", ASME Journal of Vibration and Acoustics, Vol.116, No.3, pp.341-349, 1994.

3. Van Nostrand, W.C. and Inman, D.J., "Finite Element Model for Active Constrained Layer Damping", Proceedings of the 31st Society of Engineering Science Meeting, October 1994, SPIE Vol.2427, Active Materials and Smart Structures, G.L. Anderson and D.C. Lagoudas, Eds. pp.124-139.

4. Rongong, J.A., Wright, J.R., Wynne, R.J. and Tomlinson, G.R., "Modeling of a Hybrid Constrained Layer/Piezoceramic Approach to Active Damping", ASME Journal of Vibration and Actoustics, Vol.119, pp.120-130, 1997.

5. Shi, Y.M., Li, Z.F., Hua, H.X. and Fe, Z.F., "The Modeling and Vibration Control of Beams with Active Constrained Layer Damping", Journal of Sound and Vibration, Vol.245, No.5, pp.785-800, 2001.

6. Balamurugan, V. and Narayanan, S., "Finite Element Formulation and Active Vibration Control Study on Beams using Smart Constrained Layer Damping (SCLD) Treatment", Journal of Sound andVibration, Vol.249, No.2, pp.227-250, 2002.

7. Lim, Y.H., Varadan, V.V. and Varadan, V.K., "Closed Loop Finite Element of Modeling of Active Constrained Layer Damping in the Time Domain Analysis", Journal of Smart Materials and Structures, Vol.11, pp.89-97, 2002.

8. Liao, W.H. and Wang, K.W., "Characteristics of Enhanced Active Constrained Layer Damping Treatments with Edge Elements, Part-1 : Finite Element Model Development and Validation", ASME Journal of Vibration and Acoustics, Vol.120, pp.886-893, 1998.

9. Badre-Alam, A., Wang, K.W. and Gandhi, F., "Optimization of Enhanced Active Constrained Layer (EACL) Treatment on Helicopter Flexbeams for Aeromechanical Stability Augmentation", Journal of Smart Materials and Structures, Vol.8, pp.182-196, 1999.

10. Lam, M.J., Inman, D.J. and Sunders, W.R., "Vibration Control Through Passive Constrained Layer Damping and Active Control", Journal of Intelligent Material Systems and Structures, Vol.8, No.8, pp.663-677, 1997.

11. Garg, D.P. and Anderson, G.L., "Structural Vibration Suppression via Active/Passive Techniques", Journal of Sound and Vibration, Vol.262, No.3, pp.739-751, 2003.

12. Golla, D.F. and Hughes, P.C., "Dynamics of Viscoelastic Structures - A Time-Domain, Finite Element Formulation", ASME Journal of Applied Mechanics, Vol.52, pp.897-906, 1985.

13. McTavish, D.J. and Hughes, P.C., "Modeling of Linear Viscoelastic Space Structures", ASME Journal of Vibration and Acoustics, Vol.115, pp.103-110, 1993.

14. Christensen, R.M., "Theory of Viscoelasticity : An Introduction, 2nd Ed., Academic Press, Inc., New York, 1982.

15. Crawley, E.F. and De, Luis, J., "Use of Piezoelectric Actuators as Elements of Inielligent Structures", AIAA Journal, Vol.25, No.10, pp.1373-1385, 1987.

16. Sun, D. and Mills, J.K., "PZT Actuator Placement for a Structural Vibration Damping of High Speed Manufacturing Equipment", Proceedings of the American Control Conference, 1999, San Diego, California, USA.